ELSEVIER

J. Non-Newtonian Fluid Mech. 122 (2004) 107–116

Journal of Non-Newtonian Fluid Mechanics

www.elsevier.com/locate/jnnfm

On the occurrence of even harmonics in the shear stress response of viscoelastic fluids in large amplitude oscillatory shear

Kunt Atalık[a], Roland Keunings[b,*]

[a] *Mechanical Engineering Department, Boğaziçi University, 34342 Bebek, Istanbul, Turkey*
[b] *CESAME, Division of Applied Mechanics, Batiment Euler, Université catholique de Louvain, B-1348 Louvain-la-Neuve, Belgium*

Received 4 July 2003; received in revised form 31 October 2003; accepted 3 November 2003

This article is part of a Special Volume containing papers from the XIIIth International Workshop on Numerical Methods in Viscoelastic Flows

Abstract

The non-linear response of polymeric liquids observed experimentally in large amplitude oscillatory shear (LAOS) is generally characterized by the presence of odd harmonics of the excitation frequency in the Fourier spectrum for the shear stress. Even harmonics of relatively smaller amplitude have also been observed, whose appearance is usually attributed to wall slip phenomena. In the present work, we show that wall slip is not a necessary condition for the occurrence of even harmonics. To this end, we perform a non-linear study of planar LAOS flow between two infinite parallel plates using either a monotone or non-monotone viscoelastic constitutive equation (i.e., respectively, the Giesekus and Johnson–Segalman models). The analysis allows for spatially non-homogeneous velocity and stress fields. We assume no-slip boundary conditions, and investigate the combined effects of inertia, elasticity, and shear thinning by means of spectral methods. A regular perturbation analysis is also conducted in the inertialess monotone case. Results for the Giesekus model show that combination of elasticity and shear thinning yields transient even harmonics in shear stress whose life span and intensity are considerably increased by inertia. Furthermore, the one-dimensional flow is unstable to finite two-dimensional perturbations under inertia and at high elasticity. This results in the development of secondary flows and saturation of even harmonics into small but finite values. Simulations for the non-monotone Johnson–Segalman model predict even harmonics of relatively larger amplitude that settle in dynamic equilibrium. Furthermore, the fluid's response is quasi-periodic with the appearance of incommensurate frequencies.

Keywords: Large amplitude oscillatory shear; Fourier transform rheology; Non-linear stability; Spectral methods

1. Introduction

Experimental studies of large amplitude oscillatory shear (LAOS) flows of polymer melts show non-linear effects yielding multi- and quasi-periodic behaviour in certain parameter ranges [1,2]. Fourier analysis of the shear stress response indicates that multi-periodicity manifests itself mainly with the presence of odd harmonics of the fundamental excitation frequency. In many cases, however, even harmonics of much smaller amplitude than the odd ones have also been observed [1,3–5]. Theoretical and numerical studies have been carried out to investigate these non-linear effects. In a study using single and multi-mode upper-convected Maxwell (UCM) and Oldroyd-B models [6], no bifurcation has been detected and the system's steady response has been found to be one-periodic. In recent studies [4] with simple non-Newtonian models (even inelastic), the excitation of the odd harmonics of the fundamental frequency has been demonstrated. The presence of even harmonics and higher-order bifurcations has been attributed to wall slip phenomena [7–9], and use of dynamic wall slip (memory slip) models led to a chaotic response with a continuous energy spectrum [10,11]. Recently, the effects of inertia on the formation of even harmonics have been investigated through the UCM model supplemented with a kinetic rate equation, and the authors reported that inertia does not create even harmonics [12].

In the present study, we investigate whether even harmonics in the shear stress spectrum can possibly occur in LAOS flows when no-slip boundary conditions are assumed. We

* Corresponding author. Tel.: +32 10 47 2087; fax: +32 10 47 2180.
E-mail address: roland.keunings@inma.ucl.ac.be (R. Keunings).

0377-0257/$ – see front matter © 2004 Elsevier B.V. All rights reserved.
doi:10.1016/j.jnnfm.2003.11.012

consider the combined effects of inertia, elasticity, and shear thinning in planar LAOS flow between two infinite parallel plates. Both monotone and non-monotone viscoelastic models (i.e., the Giesekus and Johnson–Segalman models, respectively) are considered to elucidate the generation of the harmonics. The problem is formulated in Section 2. Results assuming a known, homogeneous velocity gradient are given in Section 3. There we underline that an inelastic, non-Newtonian model with an arbitrary viscosity function can only generate odd harmonics in the shear stress spectrum. We also present a regular perturbation analysis for the Giesekus model in the inertialess regime, where the perturbation parameter is the mobility factor. It is found that shear thinning and elasticity give rise to odd and even harmonics in the shear stress spectrum, but the even harmonics appear only in transient exponentially-decaying terms. Consideration of non-homogeneous flow (assumed to be either one- or two-dimensional) requires the use of numerical techniques. In Section 4, we briefly describe the spectral methods used in this work. Results are presented in Section 5. For the monotone Giesekus model, we find that combination of elasticity and shear thinning yields transient even harmonics in shear stress whose life span and intensity are considerably increased by inertia. Furthermore, under inertia and at high elasticity, the one-dimensional flow is found to be unstable to finite two-dimensional perturbations. This non-linear instability drives two-dimensional, periodic secondary flows which produce even harmonics in the shear stress spectrum that saturate into small but finite values. For the non-monotone Johnson–Segalman model, even harmonics of relatively larger amplitude are found to settle in dynamic equilibrium and the fluid's response is quasi-periodic with the appearance of incommensurate frequencies. We conclude in Section 6.

2. Problem formulation and governing equations

We consider the planar flow of a polymer melt between two infinite parallel plates located at $y = \pm h$, where h is the channel half-width and the x and y coordinates are in the streamwise and cross-stream directions, respectively. The lower plate is fixed, while the upper plate oscillates in the x direction. The fluid is initially at rest and we specify no-slip boundary conditions at the walls. The x-component of velocity is thus set to 0 at the fixed wall, and is equal to $V_0 \cos(\omega t)$ at the oscillating wall. Here, ω is the angular frequency of excitation ($\omega = 2\pi f$, f being the frequency), and V_0 is the amplitude of excitation. The y-component of velocity vanishes at both walls. These boundary conditions amount to applying a nominal shear strain $\gamma(t) = \gamma_0 \sin(\omega t)$, where $\gamma_0 = V_0/2h\omega$, and a nominal shear rate $\dot{\gamma}(t) = \gamma_0\omega \cos(\omega t)$.

As noted previously [3], the frequency (proportional to the Deborah number) and rate of deformation amplitude (proportional to the Weissenberg number) can be varied independently in oscillatory shear flows. In order to obtain a dimensionless formulation of the problem, we select the half-width h as the length scale. Adopting $1/f$ as characteristic time scale would yield a dimensionless excitation with fixed angular frequency 2π and variable amplitude V_0/hf; the Deborah number would then appear in the problem formulation. In the present work, we select instead the ratio h/V_0 as the time scale. This choice yields a dimensionless excitation with fixed unit amplitude and variable angular frequency $\omega h/V_0$; the Weissenberg number is then used.

The conservation equations for isothermal, incompressible viscoelastic flow can be written in dimensionless form as,

$$Re\frac{D\mathbf{v}}{Dt} = -\nabla p + \beta\nabla^2\mathbf{v} + (1-\beta)\nabla\cdot\mathbf{T}, \tag{1}$$

$$\nabla\cdot\mathbf{v} = 0. \tag{2}$$

Here, $\mathbf{v}$ is the velocity vector, $\mathbf{T}$ the viscoelastic extra-stress tensor, p the pressure, and D/Dt denotes the material derivative. The dimensionless parameter β is the ratio of the 'solvent' viscosity μ_s to the total zero-shear rate viscosity $\mu = \mu_s + \mu_p$, with μ_p being the zero-shear rate polymer viscosity. The characteristic scales for the viscoelastic stress and pressure are $\mu_p V_0/h$ and $\mu V_0/h$, respectively. The Reynolds number is defined as $Re = \rho V_0 h/\mu$ where ρ is the fluid density.

In dimensionless form, the Giesekus constitutive equation reads

$$[\mathbf{I} + \alpha\, We\, \mathbf{T}]\cdot\mathbf{T} + We\,\overset{\triangledown}{\mathbf{T}} = 2\mathbf{D}, \tag{3}$$

while the Johnson–Segalman model is given by

$$\mathbf{T} + We\left[\left(1-\frac{\xi}{2}\right)\overset{\triangledown}{\mathbf{T}} + \left(\frac{\xi}{2}\right)\overset{\triangle}{\mathbf{T}}\right] = 2\mathbf{D}. \tag{4}$$

Here, $\mathbf{D}$ is the rate of deformation tensor, and the Weissenberg number is defined as $We = \lambda V_0/h$, where λ is the zero-shear rate relaxation time. The operators $\triangledown$ and $\triangle$ denote respectively the upper and lower convected derivatives,

$$\overset{\triangledown}{\mathbf{T}} = \frac{D\mathbf{T}}{Dt} - \mathbf{L}\cdot\mathbf{T} - \mathbf{T}\cdot\mathbf{L}^T, \tag{5}$$

$$\overset{\triangle}{\mathbf{T}} = \frac{D\mathbf{T}}{Dt} + \mathbf{L}^T\cdot\mathbf{T} + \mathbf{T}\cdot\mathbf{L}, \tag{6}$$

where $\mathbf{L}$ is the velocity gradient.

The viscometric response of the Giesekus and Johnson–Segalman models is detailed in [13]. The dimensionless mobility factor α controls the shear thinning behaviour of the Giesekus model (as well as its elongational response). For realistic properties, α must take values between 0 and 0.5. The constant shear viscosity UCM model is obtained with $\alpha = \beta = 0$. For $\alpha \neq 0$ and $\beta = 0$, the power-law slope of the steady shear viscosity is -1 at large shear rates. A small amount of solvent viscosity (e.g., $\beta = 0.001$) guarantees that the magnitude of the total shear stress is a monotonically increasing function of the deformation rate in steady-state shear flow. On the other hand, the Johnson–Segalman model

yields a non-monotonic shear stress versus shear rate curve for non-zero values of the slip parameter ξ and a viscosity ratio smaller than 1/9.

For $Re \neq 0$, the streamwise velocity component is an unknown non-linear function of the cross-stream coordinate. If the cross-stream velocity is assumed to vanish, the flow problem stated above is then spatially one-dimensional. We shall also consider the two-dimensional case, wherein spatially periodic solutions in the streamwise direction x are sought in a computational domain spreading over a dimensionless periodicity length L_x. In both one- and two-dimensional cases, suitable numerical methods are needed to solve the problem. These are described in Section 4.

Before discussing the numerical results, we find it useful to consider the much simpler inertialess case ($Re = 0$), wherein the velocity gradient is uniform. This we do in the following section.

3. Inertialess case

3.1. Inelastic fluid

We wish to underline first that an inelastic, non-Newtonian model with an arbitrary viscosity function can only generate odd harmonics in the shear stress spectrum.

Indeed, the shear stress T_{xy} for a general inelastic fluid is given by,

$$T_{xy} = \eta(|\dot{\gamma}|)\dot{\gamma}, \tag{7}$$

where η denotes the viscosity function with the absolute value of the shear rate $|\dot{\gamma}|$ as argument. In oscillatory shear at $Re = 0$, the dimensionless shear rate is uniform,

$$\dot{\gamma} = \frac{\cos(\omega t)}{2}. \tag{8}$$

Thus, as noted previously (e.g., [4,5]), the Fourier series of $|\dot{\gamma}|$ only involves even harmonics of the frequency 2ω. The same conclusion then also applies to the viscosity function $\eta(|\dot{\gamma}|)$. By trigonometric addition laws, the product of the viscosity function (having Fourier components of the form $\cos(2n\omega t)$) with the shear rate (proportional to $\cos(\omega t)$) can only generate odd harmonics of the fundamental frequency, i.e., terms of the form $\cos(2n\pm1)\omega t$. Hence, in the inertialess inelastic case, for any form of the viscosity function having as argument the absolute value of the shear rate, the Fourier spectrum of the shear stress only contains odd harmonics of the fundamental frequency. This shows the necessity of introducing elasticity and inertia to possibly obtain a richer spectrum.

3.2. Elastic fluid

In order to analyze the combined effects of shear thinning and elasticity, we perform a regular perturbation analysis where the stress non-linearities in the Giesekus model (3) are treated as perturbation terms. In the inertialess case, the dimensionless streamwise velocity is given by

$$u(y,t) = \frac{(1+y)\,\cos(\omega t)}{2}. \tag{9}$$

Treating the mobility factor α of the Giesekus model as a small perturbation parameter, we expand each extra-stress component as follows:

$$T_{ij} = T_{ij}^0 + \alpha T_{ij}^1 + \alpha^2 T_{ij}^2 + \cdots, \tag{10}$$

and introduce Eqs. (9) and (10) in the constitutive Eq. (3). We thus obtain a linear system of first order non-homogeneous ordinary differential equations for successive perturbation orders n of the form,

$$We\frac{\mathrm{d}T_{xx}^n}{\mathrm{d}t} + T_{xx}^n - We\,\cos(\omega t)T_{xy}^n = -We[(T_{xx}^{n-1})^2 + (T_{xy}^{n-1})^2], \tag{11}$$

$$We\frac{\mathrm{d}T_{xy}^n}{\mathrm{d}t} + \frac{T_{xy}^n - \frac{1}{2}We\,\cos(\omega t)T_{yy}^n}{2} = -We[T_{xy}^{n-1}(T_{xx}^{n-1} + T_{yy}^{n-1})] + \frac{\cos(\omega t)}{2}, \tag{12}$$

$$We\frac{\mathrm{d}T_{yy}^n}{\mathrm{d}t} + T_{yy}^n = -We[(T_{xy}^{n-1})^2 + (T_{yy}^{n-1})^2]. \tag{13}$$

The initial conditions on the stresses at each perturbation order are zero. At zeroth order, the solution has the following form,

$$\begin{aligned} T_{xx}^0 &= a_{11}^0\,\cos(2\omega t) + b_{11}^0\,\sin(2\omega t) + c_{11}^0 \\ &\quad\times \exp\left(-\frac{t}{We}\right)\sin(\omega t) + d_{11}^0\,\exp\left(-\frac{t}{We}\right) + e_{11}^0, \\ T_{xy}^0 &= a_{12}^0\,\cos(\omega t) + b_{12}^0\,\sin(\omega t) + c_{12}^0\,\exp\left(-\frac{t}{We}\right), \\ T_{yy}^0 &= 0. \end{aligned} \tag{14}$$

At order n, we have

$$\begin{aligned} T_{xx}^n(t) &= \sum_{k=0}^{2^n}[a_{11k}^n\,\cos(2k\omega t) + b_{11k}^n\,\sin(2k\omega t)] \\ &\quad + \sum_{m=0}^{2^{n+1}}\exp\left(-\frac{mt}{We}\right)\sum_{k=0}^{2^{n+1}-1} \\ &\quad\times[c_{11km}^n\,\cos(k\omega t) + d_{11km}^n\,\sin(k\omega t)], \\ T_{xy}^n(t) &= \sum_{k=0}^{2^n-1}[a_{12k}^n\,\cos(2k+1)\omega t + b_{12k}^n\,\sin(2k+1)\omega t] \\ &\quad + \sum_{m=0}^{2^{n+1}-1}\exp\left(-\frac{mt}{We}\right)\sum_{k=0}^{2^{n+1}-2} \\ &\quad\times[c_{12km}^n\cos(k\omega t) + d_{12km}^n\sin(k\omega t)], \end{aligned}$$

$$T^n_{yy}(t) = \sum_{k=0}^{2^n-1} [a^n_{22k}\ \cos(2k\omega t) + b^n_{22k}\ \sin(2k\omega t)] + \sum_{m=0}^{2^{n+1}-2} \exp\left(-\frac{mt}{We}\right) \sum_{k=0}^{2^{n+1}-3} \times [c^n_{22km}\ \cos(k\omega t) + d^n_{22km}\ \sin(k\omega t)], \quad (15)$$

where the coefficients in front of the expressions (14) and (15) are rational functions of We and ω. One observes from Eqs. (14) and (15) that the solutions are composed of decaying exponential terms, sine/cosine terms decaying exponentially in time, and sine/cosine terms which eventually define the dynamic equilibrium. In the shear stress expressions, even harmonics of the fundamental excitation frequency appear only in exponentially decaying sine/cosine terms, and the long-time solution is composed only of the fundamental frequency and its odd harmonics. In the normal stress expressions, dynamic equilibrium terms are constituted of even harmonics of the fundamental frequency, while odd harmonics appear only in exponentially decaying sine/cosine terms. We also note the absence of the fundamental excitation frequency in the dynamic equilibrium for the normal stresses. Since higher-order perturbation terms are represented in the final solution by increasing powers of the perturbation parameter, it is clear that the Fourier spectrum will be of decreasing intensity towards higher harmonics, as it can be expected. We also note that, in the exponential functions, the non-dimensional time is scaled with the Weissenberg number. Thus, if We is zero (inelastic fluid), the transient harmonics disappear, while when We is increased (higher elasticity), the corresponding terms decay more slowly. However, when shear thinning effects are absent (i.e., when the perturbation parameter α is zero), all higher harmonics in dynamic equilibrium and transient terms vanish, as it can be seen in the zeroth order solution (Eq. 14). Numerical time integration of the Giesekus model for finite α (i.e., without the perturbation assumption) confirms qualitatively the above results.

We conclude from this analysis that shear thinning and elasticity give rise (in the inertialess regime) to both odd and even harmonics in the shear stress spectrum, but the even harmonics appear only in transient exponentially-decaying terms. Consideration of the effects of inertia requires the use of numerical techniques, which we detail next.

4. Spectral methods

In the inertial case ($Re \neq 0$), the velocity field is a priori unknown and one must resort to the numerical solution of the governing equations detailed in Section 2.

For the one-dimensional problem (vanishing cross-stream velocity), we use a spectral tau method. The streamwise velocity u and viscoelastic extra-stress components T_{ij} are decomposed into Chebyshev spectral modes as follows:

$$u(y,t) = \sum_{m=0}^{M} a_m(t) T_m(y), \quad (16)$$

$$T_{ij}(y,t) = \sum_{m=0}^{M} (b_{ij})_m(t) T_m(y), \quad (17)$$

where the function $T_m(y)$ is the Chebyshev polynomial of order m, and a_m and $(b_{ij})_m$ are time dependent spectral coefficients. The above expressions are then inserted in the governing equations, which are integrated in space according to the Galerkin method of weighted residuals. A system of ordinary differential equations in time (a dynamical system) is thus obtained. In order to satisfy the no-slip boundary conditions at each time step, we drop the $(M-1)$ and M'th Galerkin equations for the velocity and replace them by the spectral versions of the boundary conditions:

$$u(-1,t) = \sum_{m=0}^{M-2} a_m(t) T_m(-1) = \sum_{m=0}^{M-2} a_m(t)(-1)^m = 0, \quad (18)$$

$$u(+1,t) = \sum_{m=0}^{M-2} a_m(t) T_m(+1) = \sum_{m=0}^{M-2} a_m(t) = \cos(\omega t). \quad (19)$$

Our simulations typically involve 50 Chebyshev modes for each unknown field. Initial values are all set to zero (rest state).

We also wish to address the stability of the one-dimensional results obtained with the monotone Giesekus model. In order to compute the evolution of finite-amplitude, two-dimensional perturbations to the one-dimensional base solutions, we adopt the streamfunction formulation used in our previous work [14] and apply periodic boundary conditions in the streamwise direction. In this case, the perturbation streamfunction and stress components are decomposed into Fourier and Chebyshev spectral modes, respectively in the streamwise and cross-stream directions, as follows:

$$\Psi(x,y,t) = \sum_{m=2}^{M} \sum_{k=-N}^{N} a_{km}(t)\ \exp\left(\frac{i2\pi kx}{L_x}\right) \Phi_m(y), \quad (20)$$

$$T_{ij}(x,y,t) = \sum_{m=0}^{M-2} \sum_{k=-N}^{N} (b_{ij})_{km}(t)\ \exp\left(\frac{i2\pi kx}{L_x}\right) T_m(y), \quad (21)$$

where a_{km} and $(b_{ij})_{km}$ are time-dependent complex coefficients which satisfy the reality condition and $\Phi_m(y)$ is a linear combination of the Chebyshev polynomials chosen to satisfy the wall boundary conditions on the perturbation part [14]. L_x is the dimensionless periodicity length in the streamwise direction. As in [14], a fully-spectral approach is used.

Our simulations typically involve 50 Chebyshev modes and 8 Fourier modes for each unknown field.

For both the one- and two-dimensional simulations, time integration is performed using a semi-implicit scheme of second order. Linear terms are integrated by the implicit Crank-Nicolson method, while all non-linear terms are integrated by the explicit Adams-Bashforth scheme.

Finally, we point out that it was not found necessary to add any artificial stress diffusion to the constitutive equations to obtain numerically stable results.

5. Inertial case: numerical simulations

We now include inertial effects for both monotone and non-monotone models. All results reported in this section are for a dimensionless frequency equal to 0.01. This value corresponds to a maximum imposed strain $\gamma_0 = 8$ that is typical of experimental conditions. Unless stated otherwise, we focus on the one-dimensional simulation results. The initial conditions for the one-dimensional case are the start-up conditions, i.e., all flow variables are set to zero initially. All numerical data are given in dimensionless form according to Section 2.

5.1. Monotone Giesekus model

The results obtained with the Giesekus fluid are for $Re = 1$. We start with the case $\alpha = 0.01$ and $We = 1$, namely very weak shear thinning and weak elasticity. As expected from previous work with constant shear viscosity UCM and Oldroyd-B fluids [6], the shear stress response is nearly one-periodic with a Fourier spectrum that shows one spike at the fundamental excitation frequency (Fig. 1). [Note that the frequencies/energies of the Fourier spectra shown in this section are usually scaled with respect to the frequency/energy of the excitation.] The corresponding shear stress–shear rate Lissajous loop is a thin ellipse as expected for a weakly elastic fluid (Fig. 2).

If we increase elasticity ($We = 10$), all other parameters being unchanged, we observe the transition to a multi-periodic response in shear stress with the appearance of the first and second odd harmonics (Fig. 3). The corresponding shear stress–shear rate loop is then a deformed ellipse (Fig. 4).

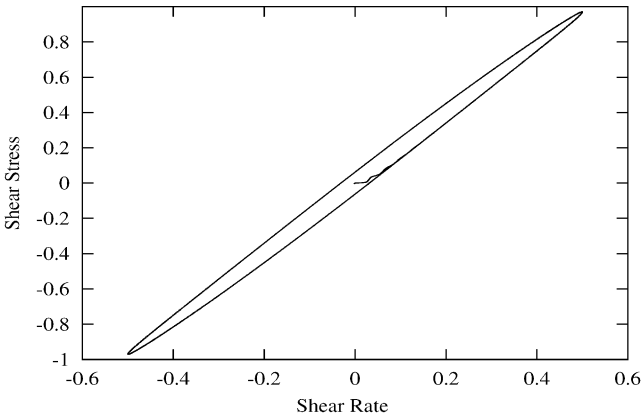

Fig. 2. Centerline shear stress vs. shear rate loop for the Giesekus model ($Re = 1$, $We = 1$, $\beta = 0.001$, $\alpha = 0.01$, $f = 0.01$).

In view of [6], if shear thinning effects were totally absent ($\alpha = 0$), the response would be one-periodic as well.

We now significantly increase shear thinning effects ($\alpha = 0.5$), all other parameters being unchanged. The net result is an increase of the multi-periodic character of the shear stress response, with the the appearance of additional odd harmonics in the Fourier spectrum (Fig. 5). Their amplitude is decreasing rapidly with increasing order.

The corresponding Lissajous plot shows secondary loops associated with the occurrence of higher-order odd harmonics (Fig. 6). For the same case, the normal stress T_{xx} has a Fourier spectrum containing even harmonics of the fundamental frequency, but not the fundamental frequency itself (Fig. 7). Here, the amplitude of the higher-order harmonics is scaled with respect to the first even harmonic. It should be noted that we also observe during an early transient phase the appearance of first even (resp. odd) harmonics of relative amplitude 10^{-3}–10^{-4} for the shear (resp. normal) stress.

Finally, we consider a situation with significant shear thinning ($\alpha = 0.2$) and high elasticity ($We = 100$). The multi-periodic evolution of the shear and normal stresses is depicted in Figs. 8 and 9, while the shear stress–shear rate loop is given in Fig. 10. It is clear that the transient phase is much longer

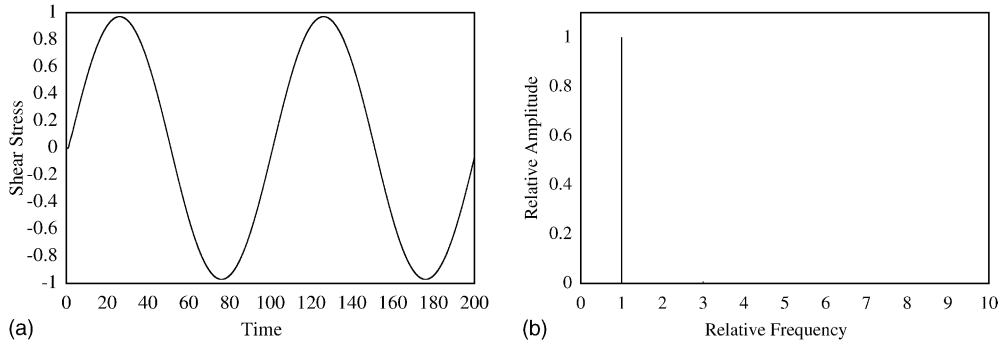

Fig. 1. (a) Evolution of shear stress at fixed plate for the Giesekus model ($Re = 1$, $We = 1$, $\beta = 0.001$, $\alpha = 0.01$, $f = 0.01$); (b) Fourier spectrum.

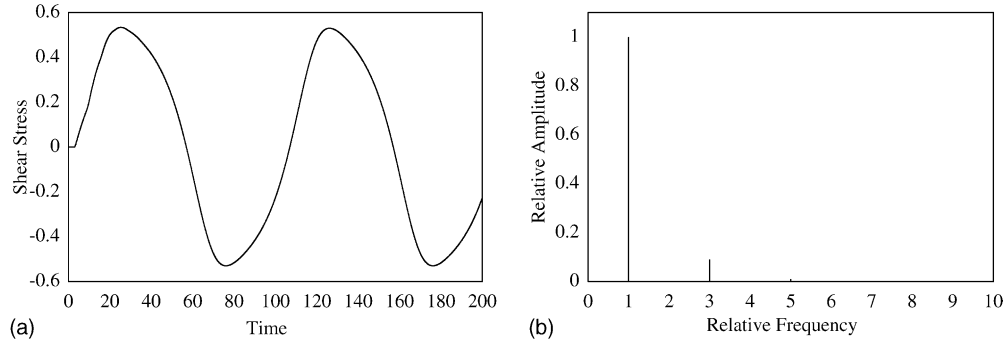

Fig. 3. (a) Evolution of shear stress at fixed plate for the Giesekus model ($Re = 1$, $We = 10$, $\beta = 0.001$, $\alpha = 0.01$, $f = 0.01$); (b) Fourier spectrum.

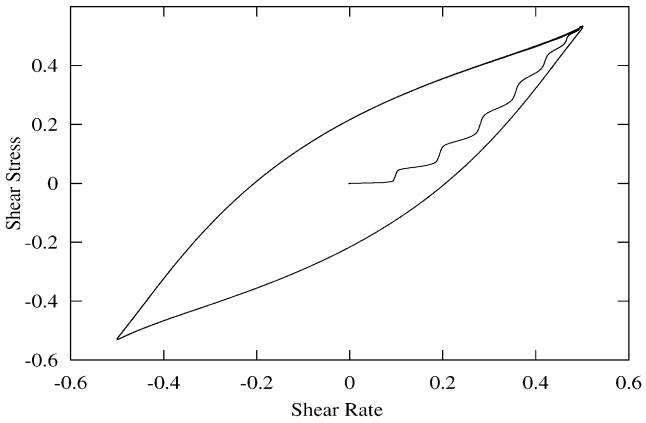

Fig. 4. Centerline shear stress vs. shear rate loop for the Giesekus model ($Re = 1$, $We = 10$, $\beta = 0.001$, $\alpha = 0.01$, $f = 0.01$).

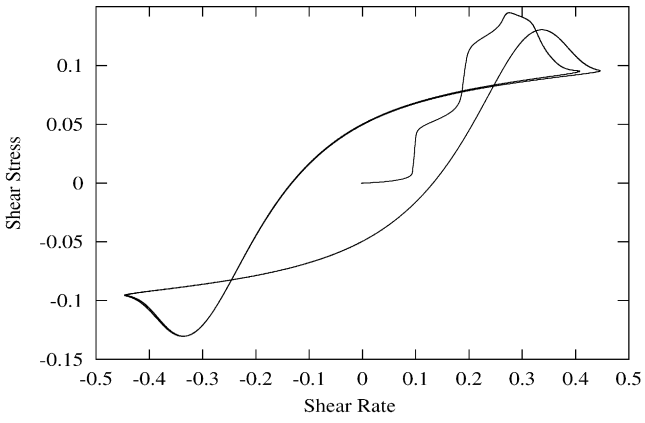

Fig. 6. Centerline shear stress vs. shear rate loop for the Giesekus model ($Re = 1$, $We = 10$, $\beta = 0.001$, $\alpha = 0.5$, $f = 0.01$).

than in the previous cases. Indeed, the long-time limit of the Lissajous plot is not fully reached in the simulation. The final behavior tends to a deformed ellipse with secondary loops.

In the present case, the even harmonics for the shear stress remain in the spectrum for much longer times (at $t = 600$, their relative amplitude is still of order 10^{-3}–10^{-4}). This can be seen in detail in Table 1. A similar observation holds for the transient odd harmonics in normal stress.

The transient behaviour of the first even harmonic of shear stress is illustrated in Fig. 11. Also shown there is the corresponding result obtained at $Re = 0$. In the latter case, the decay is very fast, in agreement with the exponential behaviour predicted in the perturbation analysis of Section 3.2. The results for $Re = 1$ show that inertial effects significantly increase both the amplitude and the life span of the first even harmonic. On the other hand, the saturation of the first odd harmonics of shear stress into a steady-state value is clearly shown in Fig. 12.

At this point, it is useful to question the stability of these one-dimensional flow results to two-dimensional perturbations. The initial conditions for the perturbation part have been formed from the eigenfunctions corresponding to the

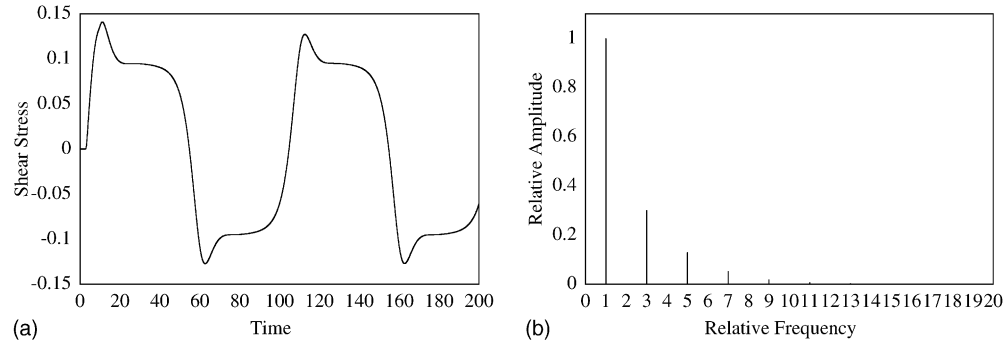

Fig. 5. (a) Evolution of shear stress at fixed plate for the Giesekus model ($Re = 1$, $We = 10$, $\beta = 0.001$, $\alpha = 0.5$, $f = 0.01$); (b) Fourier spectrum.

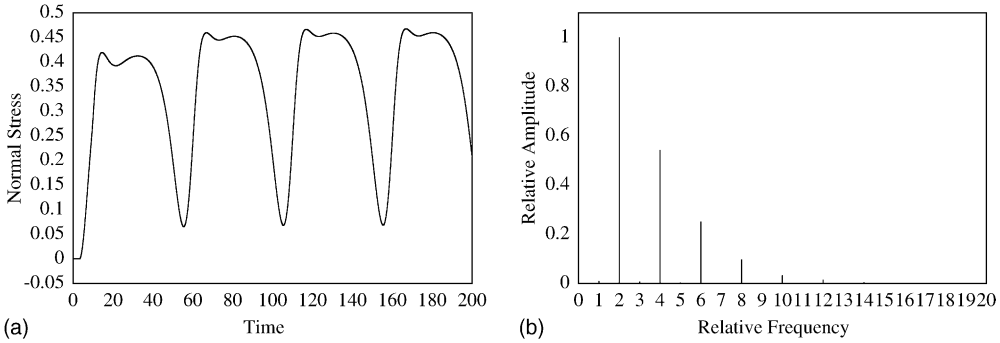

Fig. 7. (a) Evolution of normal stress at fixed plate for the Giesekus model ($Re = 1$, $We = 10$, $\beta = 0.001$, $\alpha = 0.5$, $f = 0.01$); (b) Fourier spectrum.

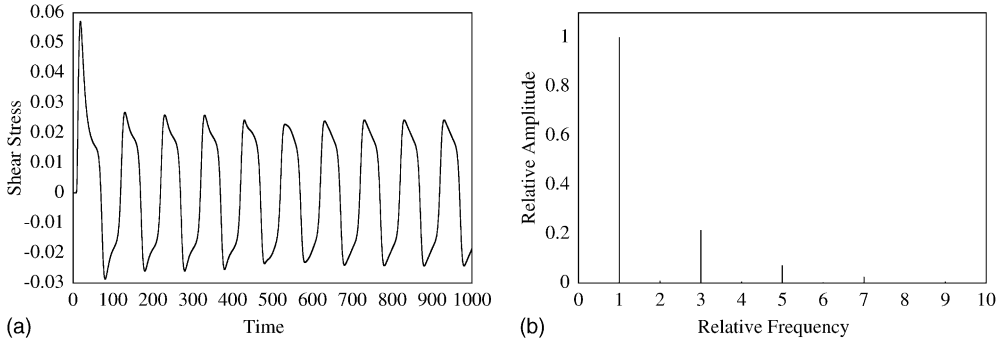

Fig. 8. (a) Evolution of shear stress at fixed plate for the Giesekus model ($Re = 1$, $We = 100$, $\beta = 0.001$, $\alpha = 0.2$, $f = 0.01$); (b) Fourier spectrum.

least stable eigenvalue of the linear stability problem. These normalized eigenfunctions are then multiplied by a perturbation factor and added to the one-dimensional solutions. Our spectral simulations indicate that the above solutions are linearly stable in the two-dimensional case, i.e., they are stable to infinitesimal two-dimensional perturbations of order 10^{-4} or less.

We then investigated the stability of the above one-dimensional solutions to two-dimensional, finite perturbations of order 10^{-3}–10^{-1}, for a streamwise periodicity length $L_x = 10$. For $Re = 1$ and $We \geq 70$, we find that the one-dimensional solution shows a non-linear instability leading to secondary flows (Figs. 13 and 14). The evolution of the stress components presents a similar multi-periodic behaviour as in the one-dimensional case. The secondary flow considerably affects, however, the Fourier spectrum: the first even harmonic in shear stress becomes pronounced and saturates into a finite value, while the first odd harmonic reaches quickly a constant value (see 2D results in Figs. 11 and 12). Upon decreasing Re below 1, we find that the secondary flow and corresponding sustained even harmonics of shear stress are suppressed. The numerical convergence of these results has been confirmed with respect to the number of Chebyshev and Fourier modes used in the simulations.

5.2. Non-monotone Johnson–Segalman model

We now briefly consider one-dimensional results obtained with the Johnson–Segalman model for $Re = 0.1$ and $We = 10$. The model parameters are set to $\xi = 0.2$ and $\beta = 0.01$.

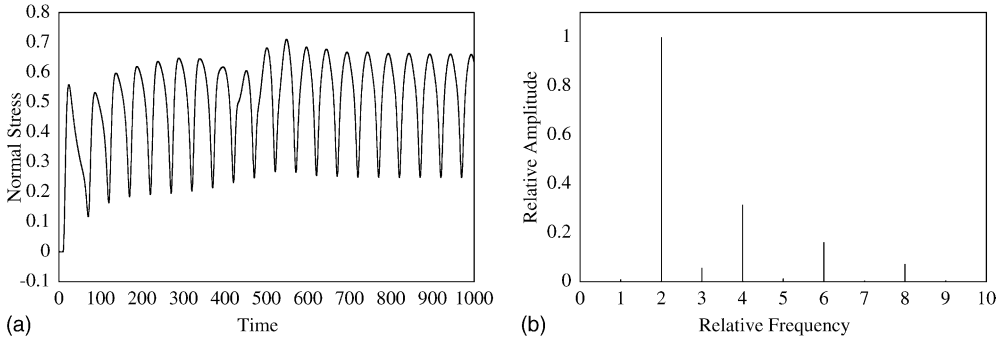

Fig. 9. (a) Evolution of normal stress at fixed plate for the Giesekus model ($Re = 1$, $We = 100$, $\beta = 0.001$, $\alpha = 0.2$, $f = 0.01$); (b) Fourier spectrum.

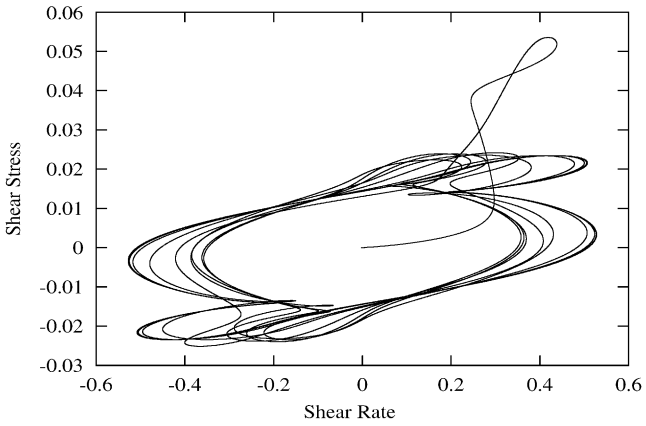

Fig. 10. Centerline shear stress vs. shear rate loop for the Giesekus model ($Re = 1$, $We = 100$, $\beta = 0.001$, $\alpha = 0.2$, $f = 0.01$).

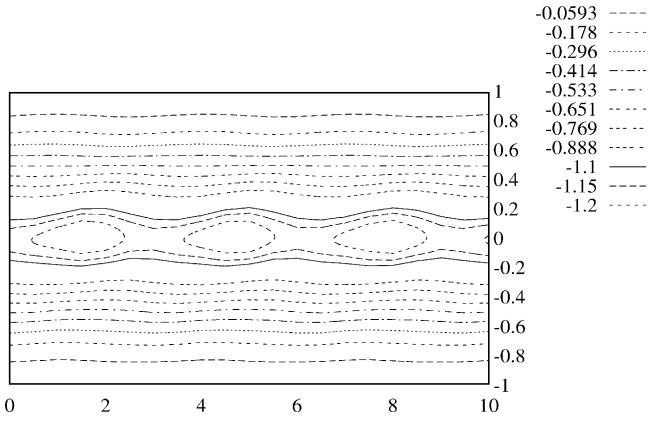

Fig. 13. Secondary flow: streamlines for the Giesekus model at $t = 700$ ($Re = 1$, $We = 100$, $\beta = 0.001$, $\alpha = 0.2$, $f = 0.01$).

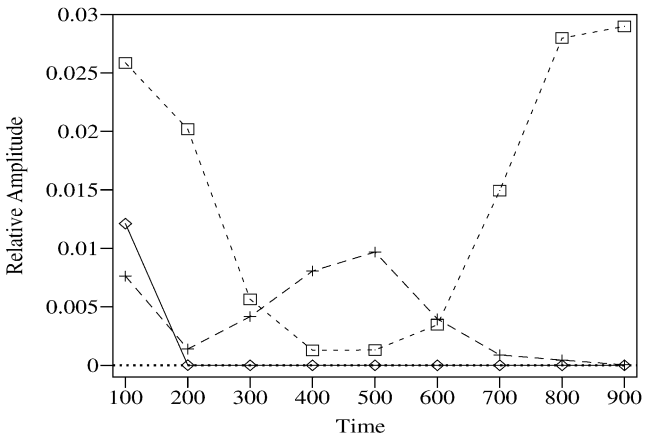

Fig. 11. Evolution of the first even harmonic of shear stress at fixed plate for the Giesekus model ($We = 100$, $\beta = 0.001$, $\alpha = 0.2$, $f = 0.01$): $Re = 0$ (△), $Re = 1$(+), $Re = 1$ (2D results) (□).

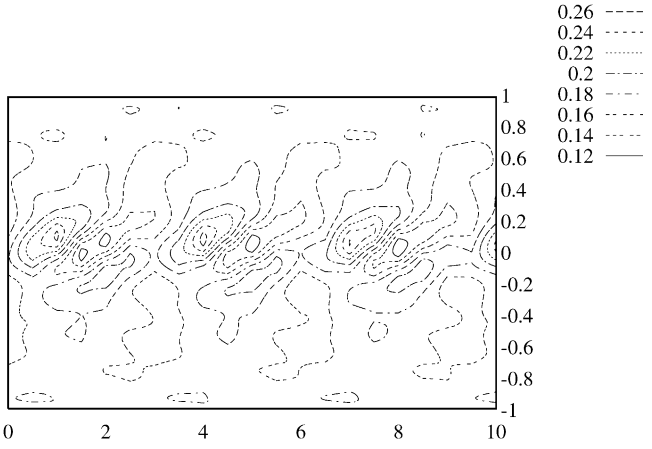

Fig. 14. Secondary flow: contour lines of shear stress for the Giesekus model at $t = 700$ ($Re = 1$, $We = 100$, $\beta = 0.001$, $\alpha = 0.2$, $f = 0.01$).

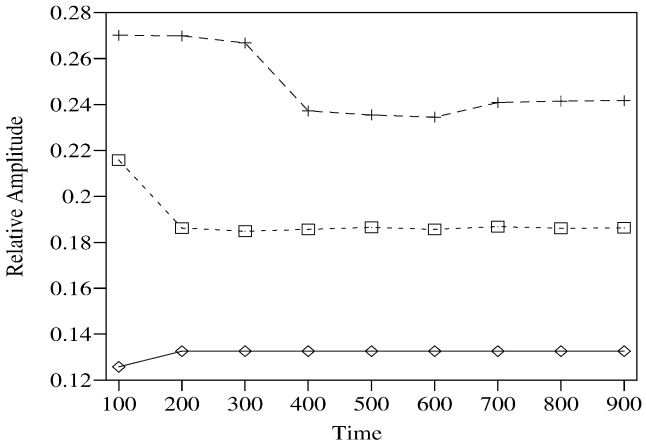

Fig. 12. Evolution of the first odd harmonic of shear stress at fixed plate for the Giesekus model ($We = 100$, $\beta = 0.001$, $\alpha = 0.2$, $f = 0.01$): $Re = 0$ (△), $Re = 1$(+), $Re = 1$ (2D results) (□).

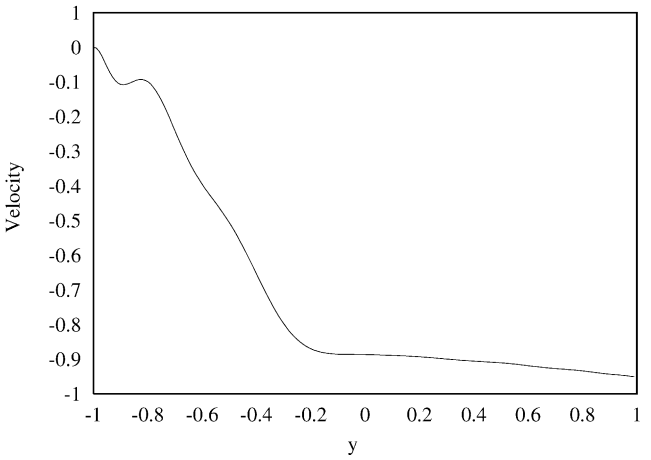

Fig. 15. Streamwise velocity distribution for the Johnson–Segalman model at $t = 360$ ($Re = 0.1$, $We = 10$, $\beta = 0.01$, $\xi = 0.2$, $f = 0.01$).

Table 1
Evolution of the relative amplitude of the harmonics of shear stress at fixed plate for the Giesekus model ($Re = 1$, $We = 100$, $\beta = 0.001$, $\alpha = 0.2$, $f = 0.01$)

Harmonic	$t = 500$–600	$t = 600$–700	$t = 700$–800	$t = 800$–900
First even	9.7×10^{-3}	4.0×10^{-3}	9.0×10^{-4}	4.5×10^{-4}
First odd	2.2×10^{-1}	2.3×10^{-1}	2.4×10^{-1}	2.4×10^{-1}
Second even	5.8×10^{-3}	2.8×10^{-3}	8.1×10^{-4}	3.8×10^{-4}
Second odd	7.3×10^{-2}	7.6×10^{-2}	7.9×10^{-2}	7.9×10^{-2}
Third even	2.7×10^{-3}	1.9×10^{-3}	4.6×10^{-4}	1.5×10^{-4}
Third odd	2.6×10^{-2}	2.4×10^{-2}	2.4×10^{-2}	2.4×10^{-2}
Forth even	2.0×10^{-3}	2.8×10^{-4}	5.6×10^{-5}	4.4×10^{-5}

Table 2
Evolution of the relative amplitude of the harmonics of shear stress at fixed plate for the Johnson–Segalman model ($Re = 0.1$, $We = 10$, $\beta = 0.01$, $\xi = 0.2$, $f = 0.01$)

Harmonic	$t = 500$–600	$t = 600$–700	$t = 700$–800	$t = 800$–900
First even	3.4×10^{-2}	5.2×10^{-2}	2.4×10^{-2}	5.3×10^{-2}
First odd	2.7×10^{-1}	3.1×10^{-1}	3.5×10^{-1}	2.9×10^{-1}
Second even	2.2×10^{-2}	2.6×10^{-2}	5.5×10^{-3}	4.8×10^{-2}
Second odd	2.0×10^{-1}	2.0×10^{-1}	2.1×10^{-1}	1.1×10^{-1}
Third even	2.4×10^{-2}	2.7×10^{-2}	2.8×10^{-2}	2.9×10^{-2}
Third odd	1.4×10^{-1}	9.7×10^{-2}	1.1×10^{-1}	1.3×10^{-1}
Forth even	2.2×10^{-2}	4.8×10^{-2}	4.0×10^{-2}	2.6×10^{-2}

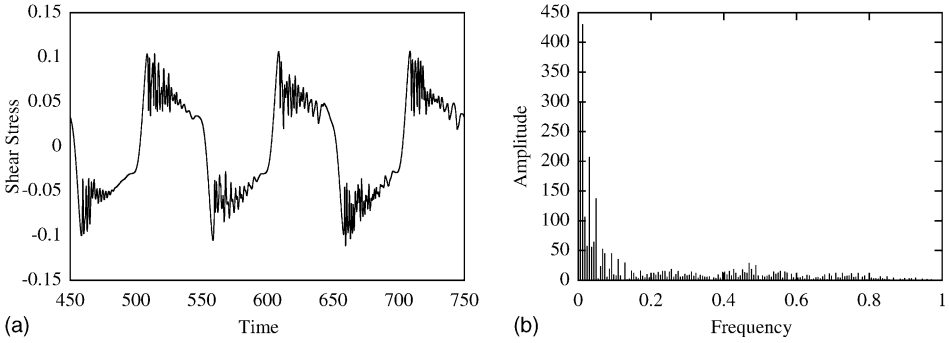

Fig. 16. (a) Evolution of shear stress at fixed plate for the Johnson–Segalman model ($Re = 0.1$, $We = 10$, $\beta = 0.01$, $\xi = 0.2$, $f = 0.01$); (b) Fourier spectrum.

In view of the non-monotone behaviour of the model, even the one-dimensional problem is numerically challenging. Indeed, the streamwise velocity component is far from having a linear profile, as can be seen in the instantaneous snapshot of Fig. 15.

The evolution of the shear stress at the fixed plate is shown in Fig. 16, together with the Fourier spectrum. Note that the amplitudes have not been scaled with the energy of the excitation frequency (the latter is the large peak located at 0.01 on the frequency axis).

The shear stress response is quasi-periodic: the Fourier spectrum contains incommensurate frequencies, in addition to odd and even multiples of the excitation frequency. Furthermore, the energy of the first even harmonic is one order of magnitude higher than in the one-dimensional results for the monotone Giesekus model, and it does not decay in time (Table 2).

Finally, the corresponding Lissajous plot is shown in Fig. 17. It clearly shows the intricacy of quasi-periodic

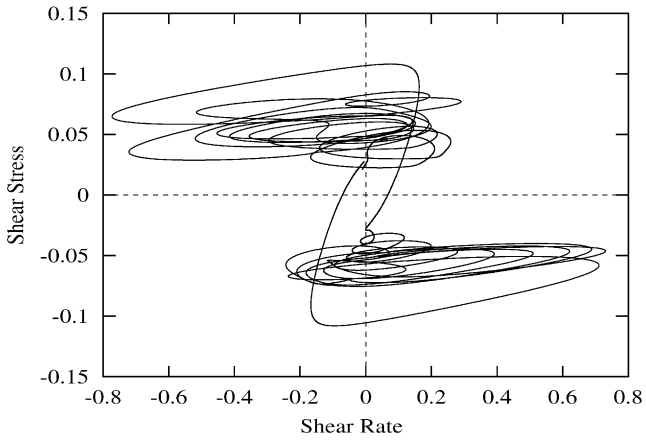

Fig. 17. Centerline shear stress vs. shear rate loop for the Johnson–Segalman model ($Re = 0.1$, $We = 10$, $\beta = 0.01$, $\xi = 0.2$, $f = 0.01$).

behaviour. Although the Lissajous plot for this case seems to be chaotic, it may be noted that it also includes part of the transitory phase of the time evolution. The quasi-periodicity of the final response can be deduced from the corresponding energy spectrum (Fig. 16) which is not continuous and decays towards high frequencies.

6. Conclusions

By performing a non-linear study of large amplitude oscillatory shear flows between two infinite plates with no-slip boundary conditions, we have shown that wall slip is not a necessary condition for the occurrence of even harmonics in the LAOS shear stress response of viscoelastic fluids. Results for the monotone Giesekus model indicate that combination of elasticity and shear thinning yields transient even harmonics in shear stress whose life span and intensity are considerably increased by inertia. Furthermore, the one-dimensional flow is found to be unstable to finite two-dimensional perturbations under inertia and at high elasticity, resulting in secondary flows and saturation of even harmonics into small but finite values. One-dimensional results for the non-monotone Johnson–Segalman model predict even harmonics of relatively larger amplitude that settle in dynamic equilibrium. Furthermore, the response is quasi-periodic with the appearance of incommensurate frequencies.

Acknowledgement

This work is supported by BASF Aktiengesellschaft and the ARC 97/02-210 project, Communauté Française de Belgique. The work of Kunt Atalık is also supported by Boğaziçi University Research Fund with project code 03HA601.

References

[1] D.W. Adrian, J.A. Giacomin, The quasiperiodic nature of a polyurethane melt in oscillatory shear, J. Rheol. 36 (1992) 1227–1243.
[2] D.W. Adrian, J.A. Giacomin, The transition to quasiperiodicity for molten plastics in large amplitude oscillatory shear, J. Eng. Mater. Tech. 116 (1994) 446–450.
[3] M.J. Reimers, J.M. Dealy, Sliding plate rheometer studies of concentrated polystyrene solutions: large amplitude oscillatory shear of a very high molecular weight polymer in diethyl phthalate, J. Rheol. 40 1 (1996) 167–186.
[4] M. Wilhelm, Fourier-Transform-Rheology, Thesis for the German Habilitation, Max-Planck-Institut für Polymerforschung, Mainz, Germany, 2000.
[5] B. Debbaut, H. Burhin, Large amplitude oscillatory shear and Fourier-transform rheology for a high-density polyethylene: experiments and numerical simulation, J. Rheol. 46 5 (2002) 1155–1176.
[6] S.A. Prost-Domasky, B. Khomami, A note on start-up and large amplitude oscillatory shear flow of multimode viscoelastic fluids, Rheol. Acta 35 (1996) 211–224.
[7] S.G. Hatzikiriakos, J.M. Dealy, Wall slip of molten high density polyethylene. I. Sliding plate rheometer studies, J. Rheol. 35 4 (1991) 497–523.
[8] S.G. Hatzikiriakos, J.M. Dealy, Role of slip and fracture in the oscillating flow of HDPE in a capillary, J. Rheol. 36 5 (1992) 845–884.
[9] M.J. Reimers, J.M. Dealy, Sliding plate rheometer studies of concentrated polystyrene solutions: nonlinear viscoelasticity and wall slip of two high molecular weight polymers in tricresyl phosphate, J. Rheol. 42 3 (1998) 527–548.
[10] M.D. Graham, Wall slip and the nonlinear dynamics of large amplitude oscillatory shear flows, J. Rheol. 39 4 (1995) 697–712.
[11] W.B. Black, M.D. Graham, Wall slip and polymer-melt flow instability, Phys. Rev. Lett. 77 5 (1996) 956–959.
[12] J.A. Yosick, J.A. Giacomin, W.E. Stewart, F. Ding, Fluid inertia in large amplitude oscillatory shear, Rheol. Acta 37 (1998) 365–373.
[13] R.B. Bird, R.C. Armstrong, O. Hassager, Dynamics of Polymeric Fluids, Fluid Mechanics, 2nd ed., vol. 1, Wiley, New York, 1987.
[14] K. Atalık, R. Keunings, Non-linear temporal stability analysis of viscoelastic plane channel flows using a fully-spectral method, J. Non-Newtonian Fluid Mech. 102 (2002) 299–319.